

Chapter 6

Exotic Force Limits [4]

Although we were unable to detect the room-temperature thermal correction with our Casimir-Polder measurement, we did clearly observe, and found good agreement with, the predicted $T = 300$ K Casimir-Polder force. Shown in Fig. 6.1 (a) is the data from our Casimir-Polder measurement (reproduced from Fig. 5.20) with only the predicted $T = 300$ K Casimir-Polder force shown. In Fig. 6.1 (b) we show the residuals if the predicted $T = 300$ K Casimir-Polder force is subtracted off of the data—clearly any additional force, if present, must be significantly smaller than the Casimir-Polder force.

We would now like to investigate what limits our Casimir-Polder measurement can set on short-range scalar-scalar Yukawa potentials that some proposed extensions to the standard model have proposed [15]. These potentials typically are written in the form:

$$U_{Yuk} = - \int dV \frac{Gm\rho}{r} (1 + \alpha e^{-r/\lambda}), \quad (6.1)$$

where G is the Newtonian constant of gravitation, m is the mass of rubidium, ρ is the density of the attracting body (in our case the fused silica substrate), r is the distance from the rubidium atom to the volume element in the substrate, α and λ parameterize the short-range Yukawa force, and the volume integral is performed over the fused silica substrate. If we set $\alpha = 0$, then we just recover the usual gravitational potential.

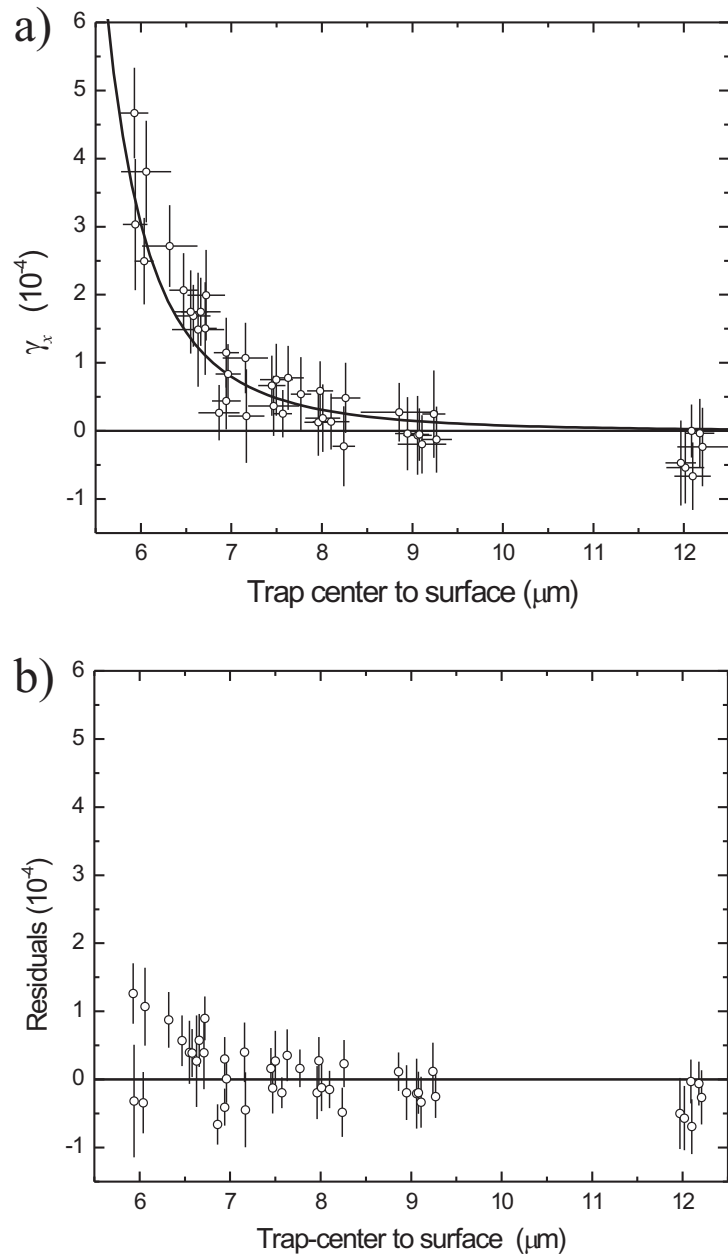


Figure 6.1: (a) The Casimir-Polder data from Fig. 5.20 with the only the predicted $T = 300$ K Casimir-Polder force shown. (b) The data from (a) with the predicted $T = 300$ K Casimir-Polder force subtracted off (we have not plotted the horizontal error bars, and the vertical error bars include only the statistical error). The *lack* of an additional forces allows us to put limits on the presence of exotic short-range forces.

In order to obtain limits on these proposed Yukawa potentials we must first convert Eq. 6.1 to a form from which we can calculate γ_x . First, we break the intergral in Eq. 6.1 into two parts:

$$U_{Yuk} = - \int dV \frac{Gm\rho}{r} - \alpha \int dV \frac{Gm\rho}{r} e^{-r/\lambda}, \quad (6.2)$$

The first term is the contribution from the gravitational attraction of the substrate and, because it is well below our experimental sensitivity, can be quite safely neglected. The integral in the second term, written in cylindrical form, is¹

$$U_{Yuk}(d) = -\alpha Gm\rho \int_0^\infty \int_d^\infty \int_0^{2\pi} r \frac{e^{-\sqrt{r^2+z^2}/\lambda}}{\sqrt{r^2+z^2}} dr dz d\theta, \quad (6.3)$$

where d is the distance between the atom and the surface of the substrate. The integral over r is simply

$$\int_0^\infty r \frac{e^{-\sqrt{r^2+z^2}/\lambda}}{\sqrt{r^2+z^2}} dr = \lambda e^{-r/\lambda}. \quad (6.4)$$

Eq. 6.2, with the r and θ integrals performed, is then

$$U_{Yuk}(d) = -2\pi\alpha\lambda Gm\rho \int_d^\infty e^{-r/\lambda} dz. \quad (6.5)$$

The final integral over z is again straightforward, and we finally obtain:

$$U_{Yuk}(d) = -2\pi\alpha\lambda^2 Gm\rho e^{-d/\lambda}. \quad (6.6)$$

Using Eq. 5.19, 6.6, and the residuals in Fig. 6.1 (b), we want to obtain a limit on the value of α for $\lambda \simeq 1-10 \mu\text{m}$. There are a number of reasonable techniques for doing this using statistical χ^2 -type arguments, but reflecting back upon our Casimir-Polder measurement, we recall that our systematic measurements played a significant

¹ Because we expect that our limits will only be significant in the $\lambda = 1-10 \mu\text{m}$ range, we can safely treat the substrate as infinite.

Table 6.1: A summary of the series systematic corrections that we apply to our Casimir-Polder data to obtain short-range force limits (only one correction is applied at a time). For each correction we list the value of α that was obtained by fitting to the residuals (for systematic corrections that occur in positive and negative directions we list the largest magnitude α value obtained). *These are not “fractional” corrections, instead these numbers refer to absolute corrections in the normalized frequency shift γ_x .

Uncertainty Source	Size (1σ)	Direction	Fit α ($\lambda = 2\mu\text{m}$)
Magnification	1.3%	$\pm d$	8.4×10^{10}
Oscillation Amplitude	2.2%	$\pm a$	5.1×10^{10}
Thomas-Fermi Radius	2.0%	$\pm R_x$	4.8×10^{10}
Spatial Inhomogeneity	$\sim 2.5 \times 10^{-5}*$	$-\gamma_x$	-4.4×10^{10}
Uniform Magnetic	$\sim 2.2 \times 10^{-5}*$	$\pm\gamma_x$	14.0×10^{10}
Uniform Electric	$\sim 0.4 \times 10^{-5}*$	$-\gamma_x$	-2.0×10^{10}

role in the uncertainty of our data. Thus, the uncertainty in one of our systematics will dominate our limit on short-range forces.

For each of our systematic uncertainties [listed in Table 6] we shift our data, or the predicted Casimir-Polder force for the “Oscillation Amplitude” and the “Thomas-Fermi Radius” corrections, by twice the uncertainty (or 2σ). This corresponds approximately to the 95% uncertainty for that systematic. Then using the shifted data, or predicted Casimir-Polder force, we calculate a new set of residual data. Using this residual data (with weighting provided by the statistical error bars, as are shown in Fig. 6.1 (b)), and assuming an surface potential of the form of Eq. 6.6, we fix λ to a value between 100 nm and 10 μm , and then fit α to the residuals. That α value then represents the largest short-range force, for that particular value of λ , that is consistent with our 95% uncertainty in that particular systematic. We repeat this for each of the systematics listed in Table 6.1 and then take the largest value of $|\alpha|$ at each value of λ to be our 95% limit for short-range forces.

For example, let’s review the uniform magnetic systematic uncertainty, which turns out to dominate the force limit.

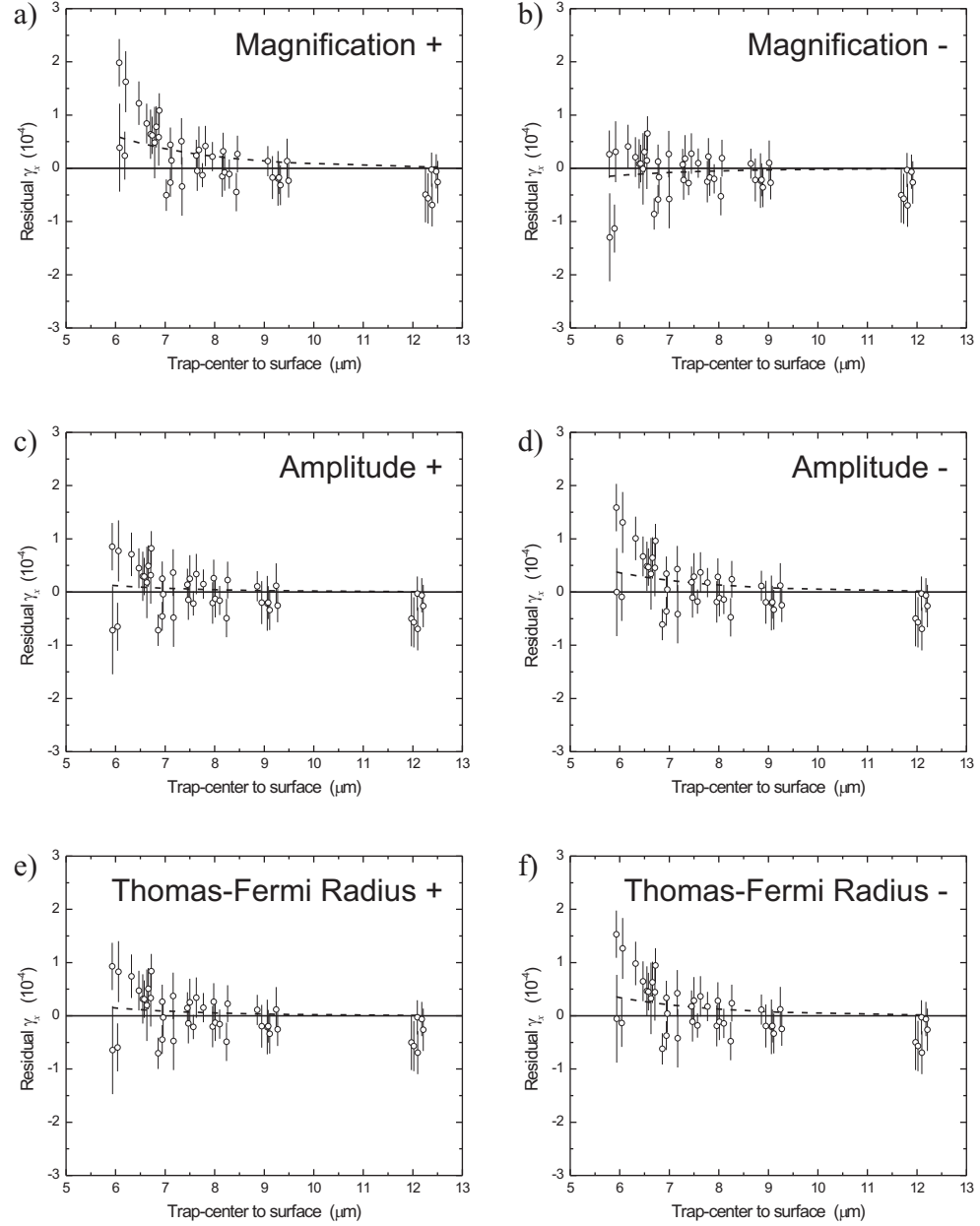


Figure 6.2: The obtained residual γ_x after the predicted $T = 300$ K Casimir-Polder force has been subtracted off. (a) and (b) The positive and negative $2\text{-}\sigma$ adjustment of the magnification. This shifts the data points along the horizontal axis. (c) and (d) The positive and negative $2\text{-}\sigma$ adjustment of the dipole oscillation amplitude. This only shifts the predicted Casimir-Polder force upwards and downwards. (e) and (f) The positive and negative $2\text{-}\sigma$ adjustment of the Thomas-Fermi radius in the \hat{x} -direction. Again, this only shifts the predicted Casimir-Polder force upwards and downwards.

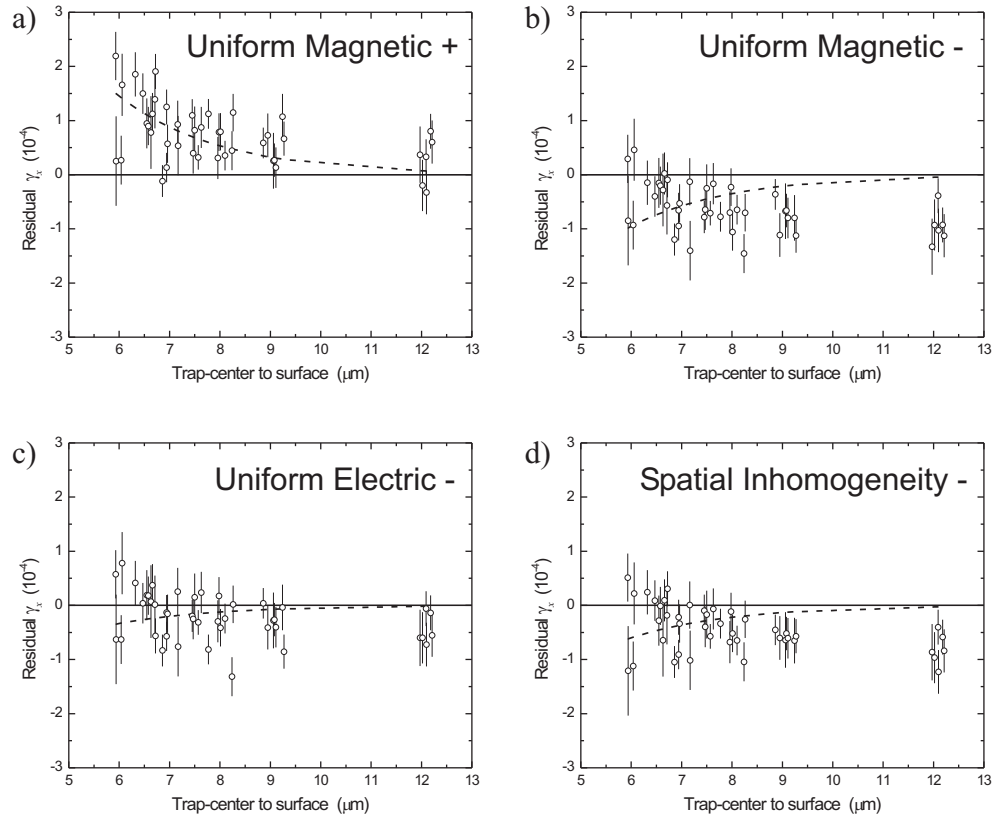


Figure 6.3: The obtained residual γ_x after the predicted $T = 300$ K Casimir-Polder force has been subtracted off. (a) and (b) The addition and subtraction of $2\times$ the uniform magnetic systematic uncertainty. This moves the data points upwards and downwards. (c) The subtraction of $2\times$ the uniform electric systematic uncertainty. We only subtract this uncertainty because electric fields are always attractive. This moves the data points downwards. (d) The subtraction of $2\times$ the spatially inhomogeneous systematic uncertainty. Again, we only subtract this uncertainty because the spatially inhomogeneous forces we encountered are generated by electric fields.

Twice systematic uncertainty as calculated from Eq. 5.38,² which was individually determined for each data point, is added or subtracted (corresponding to attractive or repulsive magnetic surface forces) to each data point. This represents the 95% confidence limits for the presence of attractive or repulsive magnetic forces. The predicted $T = 300$ K Casimir-Polder force is then subtracted to create the residual normalized

² In fact, rather than add the terms in quadrature as is done in the equation we directly added them directly. This was done to calculate a *worst-case* magnetic systematic limit.

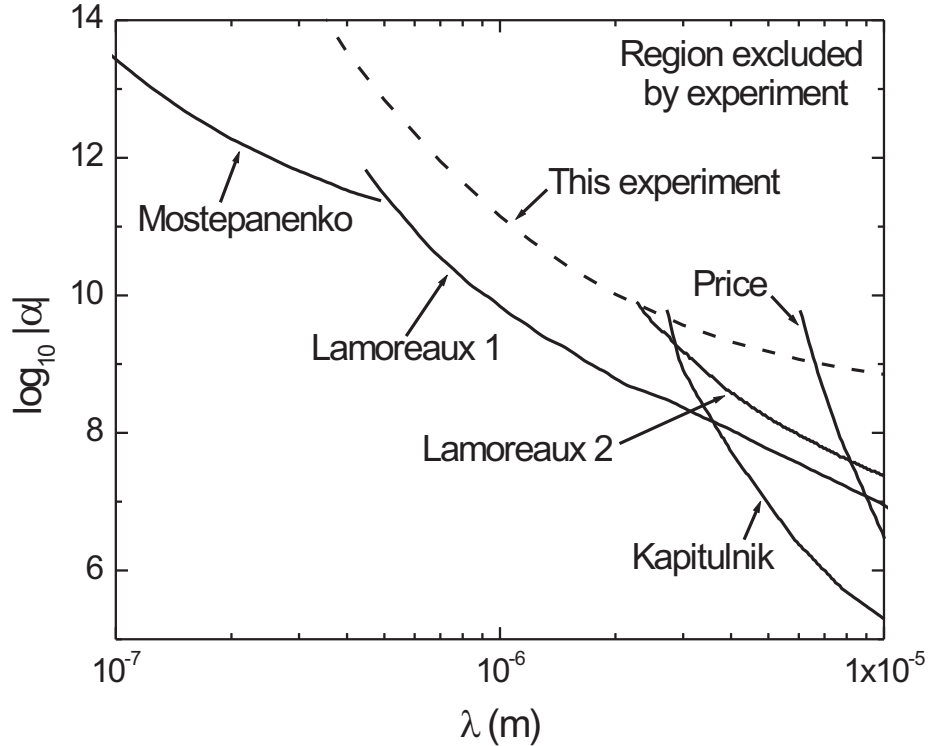


Figure 6.4: Current short-range Yukawa-type force limits in the 0.1–10 μm range. The limits obtained from this experiment are shown by the dashed line. The limits labelled Mostepanenko, Kapitulnik, and Price are from [72], [73], and [74], respectively. The limits labelled Lamoreaux (a) and (b), from [75] and [76], respectively, are from two different analyses of the Lamoreaux experiment [71].

frequency shifts, and α is fit to the residual data for a range of λ values to obtain the limit curve. In Fig. 6.2 and Fig. 6.3 the residual normalized frequency shifts for each of the systematic uncertainties listed in Table 6.1 is shown. Finally, for each value of λ , we take the largest value of $|\alpha|$ obtained from *any* of the systematic uncertainties as our limit.

The limit obtained using this technique is plotted in Fig. 6.4 with the current experimental limits in this region. Redesigning the experiment to optimize sensitivity

to this signal could permit over an order of magnitude improvement in the short-range force sensitivity. This improvement could be accomplished by, for instance, using a material with significantly higher density,³ or by working over a surface where the condensate extends over two materials of different density.⁴

³ If the alkali adsorbate issues could be resolved then a conductive material such as rhenium could be used. The density of rhenium is almost an order of magnitude larger than the density of fused silica.

⁴ Working over materials two materials with different density that generate similar a Casimir-Polder force avoid complications related to the subtraction of the Casimir-Polder as was necessary for this analysis.